Journal of the Physical Society of Japan
Vol. 68, No. 3, March, 1999, pp. 716-719

Conductance of Carbon Nanotubes with a Vacancy

Masatsura IGAMI, Takeshi NAKANISHI[1] and Tsuneya ANDO[2]

Institute of Materials Science, University of Tsukuba, 1–1–1 Tennodai, Tsukuba-shi, Ibaraki 305-8573
[1]*Institute of Physics and Chemical Research (RIKEN), 2–1 Hirosawa, Wako-shi, Saitama 351-0198*
[2]*Institute for Solid State Physics, University of Tokyo, 7–22–1 Roppongi, Minato-ku, Tokyo 106-8666*

(Received December 8, 1998)

The conductance of carbon nanotubes with a vacancy is studied in a tight-binding model. We examine the Fermi energy ϵ dependence of the conductance and show it is quantized into zero, one, and two times the conductance quantum $e^2/\pi\hbar$ depending on the type of vacancy in the half-filled case, i.e., $\epsilon = 0$. In the presence of a magnetic field, the conductance is scaled by the component of the magnetic field in the direction of the vacancy.

KEYWORDS: graphite, carbon nanotube, Fullerene tube, topological disorder, magnetoconductance, recursive Green's function technique, Landauer's formula, mesoscopic system

Carbon nanotubes (CN's) were first discovered by Iijima in 1991.[1)] They consist of coaxially rolled graphite sheets and their electronic states change critically from metallic to semiconducting depending on their tubular circumferential vector.[2-5)] Because of the peculiarity of their geometric and electronic structure, they provide a new kind of quantum wire. The purpose of this work is to study the effects of scattering by a vacancy in metallic armchair nanotubes in the presence and absence of a magnetic field.

Recently, the conductivity of CN's with impurity potential was studied and it was proved that the Born series for back-scattering vanish identically for scatters having a potential range larger than the lattice constant.[6)] This intriguing fact was related to Berry's phase acquired by a rotation in the wave-vector space in the system described by a $\mathbf{k}\cdot\mathbf{p}$ Hamiltonian, which is the same as Weyl's equation for a neutrino.[7)] This was confirmed by a tight-binding calculation.[8)] There have been some reports on experimental studies of transport in CN bundles.[9)] Measurements of magnetotransport of a single nanotube became possible,[10, 11)] and quantized conductance in a multi-wall nanotube has been reported.[12)]

Some recent experiments suggest the existence of defective nanotubes of carpet-roll or papier-mâché forms.[13, 14)] These systems have many disconnections of the π electron network governing the transport of CN's, and therefore are expected to exhibit properties different from those in perfect CN's. In fact, the effects of topological defects, i.e., five- or seven-member rings, in nanotube junctions have been calculated and a universal power-law dependence on the conductance was shown.[15-17)] A calculation of the conductance of armchair nanotubes with a single vacancy has also been reported.[18)]

We use a tight-binding model of a single π band with a nearest-neighbor hopping integral γ_0 and a lattice constant a. A magnetic field is introduced through a Peierls phase factor.[19, 20)] The armchair nanotube is known to always be metallic and to have two bands in the vicinity of the Fermi energy crossing at $k_y = 2\pi/3a$ (K point) and $k_y = -2\pi/3a$ (K' point). The energy dispersion near the Fermi energy is approximately given by $\epsilon = \gamma k$, where k is the wave vector measured from the K and K' points and $\gamma = \sqrt{3}a\gamma_0/2$. Two channels denoted as K and K' with positive velocity $\gamma/\hbar$ have the dispersion $\epsilon = +\gamma k$ and two with negative velocity $-\gamma/\hbar$ have $\epsilon = -\gamma k$.

A unit cell of two-dimensional graphite contains two carbon atoms denoted A and B constituting a honeycomb network, as shown in Fig. 1. We consider three typical vacancies: (a) vacancy I, (b) vacancy IV, and (c) vacancy II. In vacancy I a single carbon site (site A) is removed, in vacancy IV three A sites and one B site are removed, and in vacancy II a pair of A and B sites are removed.

The vacancies are simulated by two models. In the first model, we consider the explicit disconnection of bonds around the vacancy. In the second model, a huge on-site energy ($\simeq\gamma_0 \times 10^8$) is introduced at vacancy sites on the perfect network of CN's. Because the calculated conductance for both models agree with each other within numerical accuracy, we can conclude that these two models are equivalent.

A magnetic field perpendicular to the tube axis leads to various peculiar electronic properties of CN's including transport.[21-23)] It is characterized by strength H as well as angle θ_H from the direction pointing from the center to the vacancy [see the inset of Fig. 4]. The effective strength of the field is characterized by $(L/2\pi l)^2$, where L is the circumference of CN's and l is the magnetic

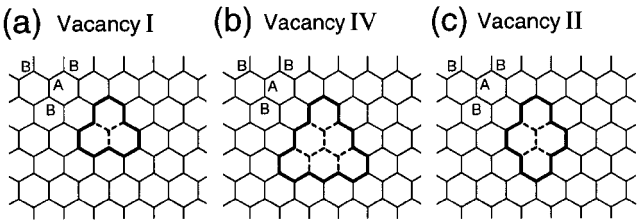

Fig. 1. Three typical vacancies. We call the vacancies depicted in (a), (b), and (c) vacancy I, IV and II, respectively.

length given by $l = \sqrt{c\hbar/eH}$.[5] We have two regimes, the weak-field regime $(L/2\pi l)^2 \ll 1$ and the strong-field regime $(L/2\pi l)^2 \gg 1$. In the former case, the wave function is extended almost uniformly along the circumference. In the latter case, Landau levels are formed in the vicinity of $\epsilon = 0$ and corresponding wave functions are localized at the top and the bottom of CN in the direction of the magnetic field.

Transmission $t_{\mu\nu}$ and reflection coefficients $r_{\mu\nu}$ are calculated by a recursive Green's function technique,[24, 25] where μ and ν are out-going and in-coming channels, respectively. The unitarity of the scattering matrix must be carefully checked throughout the numerical calculations. The conductance is calculated by the multichannel Landauer's formula,[26] given by

$$G = \frac{e^2}{\pi\hbar} \sum_{\mu,\nu} |t_{\mu\nu}|^2. \tag{1}$$

In the following, we shall exclusively consider the case that $-\epsilon(1) < \epsilon < \epsilon(1)$, where $\epsilon(1)$ is the bottom of the second conduction bands. In this case, the conduction and valence bands having a nearly linear dispersion contribute to traveling channels, and combinations of $\{\mu, \nu\}$ are given by $\{\mathrm{K}, \mathrm{K}\}$, $\{\mathrm{K}', \mathrm{K}'\}$, $\{\mathrm{K}', \mathrm{K}\}$, and $\{\mathrm{K}, \mathrm{K}'\}$. The former two correspond to intra-valley scattering and the latter two to inter-valley scattering between K and K' points. We have $G = 2e^2/\pi\hbar$ in perfect nanotubes. Furthermore, all the results are symmetric with respect to $\epsilon = 0$ because of the electron-hole symmetry. For sufficiently thick CN's, i.e., $L/a \gg 1$, we have $\epsilon(1) = 2\pi\gamma/L$. If we adopt $\gamma_0 = 3.03\,\mathrm{eV}$ and $a = 2.46\,\text{Å}$, we have $\epsilon(1) \simeq 0.94\,\mathrm{eV}$ and $0.16\,\mathrm{eV}$ for $L = 42.6\,\text{Å}$ and $256\,\text{Å}$, respectively.

Figure 2 shows the calculated conductance as a function of the Fermi energy. For the vacancy I, the conductance at $\epsilon = 0$ is half that in a defect-free system as shown in Fig. 2(a). Both intra- and inter-valley components have equal amplitude for both transmission and reflection processes, i.e., $|t_{\mu\nu}|^2 = |r_{\mu\nu}|^2 = 1/4$. The conductance increases as a function of ϵ for $0 < \epsilon < \epsilon(1)$ and reaches $2e^2/\pi\hbar$ at $\epsilon = \epsilon(1)$, where a perfect transmission occurs, i.e., $|t_{\mathrm{KK}}| = |t_{\mathrm{K'K'}}| = 1$. Except at $\epsilon = 0$ and $\epsilon = \epsilon(1)$, the conductance increases with the increase of the circumference.

Effects of the vacancy I in armchair nanotubes were studied in a similar tight-binding model,[18] in which the conductance at $\epsilon = 0$ was claimed to approach $2e^2/\pi\hbar$ with increasing L. It is likely, however, that the results do not exactly correspond to $\epsilon = 0$ but to a small, nonzero value. In fact, if we plot the calculated conductance against L for $\epsilon/\gamma_0 = 0.02$, we get a curve almost the same as that given in Fig. 3 of ref. 18.

In CN's with vacancy IV, the conductance at $\epsilon = 0$ vanishes, as shown in Fig. 2(b) and a perfect reflection occurs within the same valley, i.e., $|r_{\mathrm{KK}}| = |r_{\mathrm{K'K'}}| = 1$. The conductance increases with increasing ϵ and reaches $2e^2/\pi\hbar$ at $\epsilon = \epsilon(1)$. Except at $\epsilon = 0$ and $\epsilon = \epsilon(1)$, the conductance increases with increasing L.

In CN's with vacancy II, the conductance around $\epsilon = 0$ is slightly smaller than $2e^2/\pi\hbar$ and gradually increases and approaches $2e^2/\pi\hbar$ with the increase of the radius,

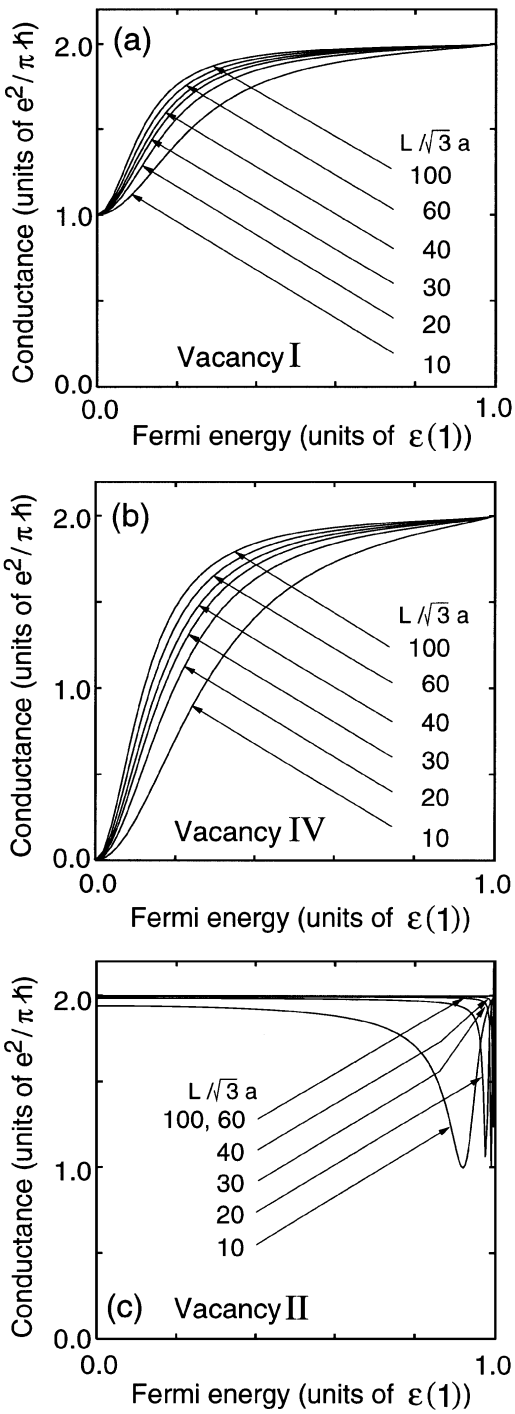

Fig. 2. Calculated conductance in units of $e^2/\pi\hbar$ as a function of the Fermi energy for CN's with vacancy I (a), IV (b), and II (c), where the energy is scaled by $\epsilon(1)$, which corresponds to the bottom of the second conduction bands.

as shown in Fig. 2(c). The deviation from perfect conductance $2e^2/\pi\hbar$ decreases with increasing L almost in proportion to L^{-2}. For example, magnitude of total reflection coefficients at $\epsilon = 0$ is 3.7×10^{-3} and 0.6×10^{-3} for $L/\sqrt{3}a = 40$ and 100, respectively. The conductance exhibits a dip at the energy slightly below $\epsilon = \epsilon(1)$, but reaches $2e^2/\pi\hbar$ at $\epsilon = \epsilon(1)$. The back scattering within each valley r_{KK} and $r_{\mathrm{K'K'}}$ and the transmission between different valleys $t_{\mathrm{KK'}}$ and $t_{\mathrm{K'K}}$ are absent because of a mirror symmetry about a plane containing the axis.[17]

Energy levels associated with vacancy II can be calculated using a super-cell method in which we consider

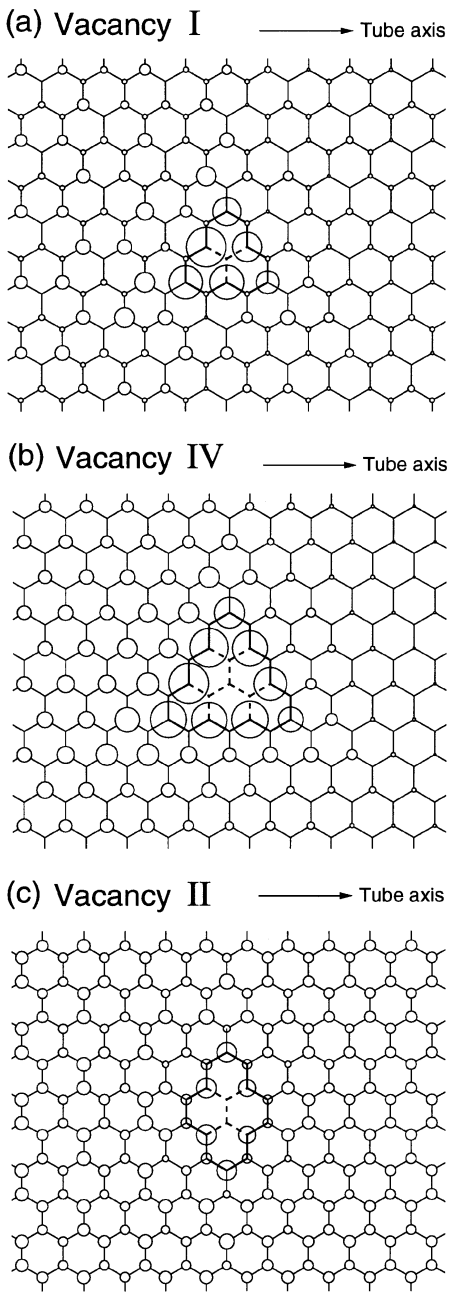

Fig. 3. The density distribution of a wave at $\epsilon = 0$ incident from the left-hand side in the K-valley around the vacancy I (a), IV (b), and II (c) for $L/\sqrt{3}a = 10$. The radius of a circle at each lattice point is proportional to the magnitude of the electron density.

a finite-length nanotube and impose periodic boundary conditions. The results show the presence of a localized state slightly below the bottom of the second conduction band. The dip slightly below $\epsilon = \epsilon(1)$ is likely to be due to resonance scattering from such a localized level.

The qualitative difference of calculated conductance at $\epsilon = 0$ is clearly reflected in the wave function around the vacancy. We depict the calculated density distribution around the vacancy for a wave incident from the left-hand side in CN with $L/\sqrt{3}a = 10$, in Fig. 3 [(a) vacancy I, (b) vacancy IV, and (c) vacancy II]. Around vacancy I, the wavefunction at A sites (the vacancy is situated at an A site) has nodes with the periodicity of a three-sublattice Kekulé pattern. The wave function at B sites has a large amplitude around the vacancy. In the case of

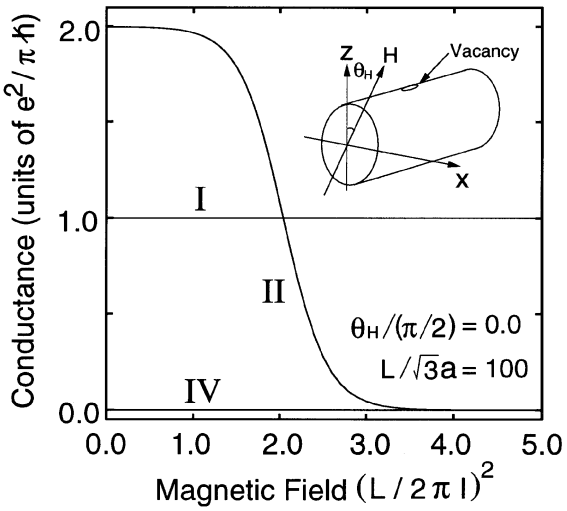

Fig. 4. Calculated conductance at $\epsilon = 0$ as a function of a magnetic field for CN's with vacancy I, IV, and II. Inset shows definition of the angle θ_H. $L/\sqrt{3}a = 100$ and $\theta_H = 0$.

vacancy IV, the wave function has no component on A sites and has a large amplitude at B sites in the left-hand side of the vacancy and a vanishingly small amplitude in the right-hand side. In the case of vacancy II, the wave function is not disturbed by the vacancy so much and the wave is almost perfectly transmitted.

The wave function is strongly perturbed by the presence of a vacancy except in the case of vacancy II. This means that evanescent waves decaying exponentially away from the vacancy play important roles. Their effects become more and more important with the increasing energy. At $\epsilon = \epsilon(1)$, in particular, the wave function given by a combination of an incident traveling mode and evanescent modes associated with the second conduction bands can be made to vanish identically in the vicinity of the vacancy. This is presumably the reason that perfect transmission is realized at $\epsilon = \epsilon(1)$. In a graphite sheet with a finite width, localized edge states are formed near the Fermi level, when the boundary is in a certain specific direction.[27-30] Such edge states might play an important role also in the case of vacancies and be closely related to the singular dependence on the type of vacancies.

Figure 4 shows the calculated conductance in magnetic fields, $\theta_H = 0$ and $L/\sqrt{3}a = 100$. It is independent of the field and remains at $e^2/\pi\hbar$ for vacancy I and zero for vacancy IV. The calculated conductance for vacancy II shows a large positive magnetoresistance, where it decreases from $2e^2/\pi\hbar$ to zero.

In the case of vacancy I, the relative importance of intra- and inter-valley scattering processes changes with the magnetic field, although not shown explicitly. In the weak field regime, both intra- and inter-valley processes occur with equal probability. In high magnetic fields, inter-valley scattering is suppressed and intra-valley transmission for in-coming channel K' and reflection for K have the same amplitude, i.e., $|t_{\mathrm{K'K'}}| \approx |r_{\mathrm{KK}}| \approx 1$. Because of the peculiar wave function in a high magnetic field,[5,23] we have $|t_{\mathrm{KK}}| \approx |r_{\mathrm{K'K'}}| \approx 1$, if a single B site is removed instead of A or $\theta_H = \pi$. In the case of vacancy IV, only intra-valley reflection is allowed

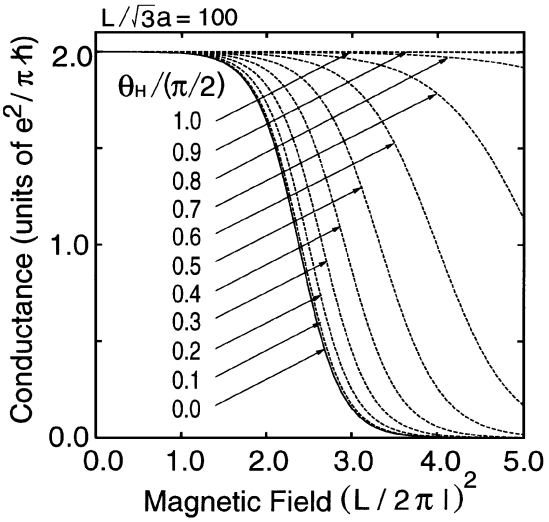

Fig. 5. Calculated conductance at $\epsilon = 0$ as a function of $(L/2\pi l)^2$ (dotted-lines) and $(L/2\pi l)^2 \cos\theta_H$ (solid lines) for the CN's with vacancy II shown in Fig. 1(c). All lines are reduced to a single common curve if plotted as a function of $(L/2\pi l)^2 \cos\theta_H$.

independent of the field.

Figure 5 shows the dependence on θ_H for vacancy II. There is no field dependence for $\theta_H = \pi/2$ and the dependence is maximum for $\theta_H = 0$. The magnetoconductance is given by a single common curve if plotted as a function of $(L/2\pi l)^2 \cos\theta_H$. This means that the conductance depends only on the field component in the direction of the vacancy.

Unfortunately, we have no intuitive picture which explains the universal dependence on $H\cos\theta_H$, but we expect that this is quite common in nanotubes. In fact, the same behavior was predicted in the magnetoconductance of CN junctions containing topological defects such as five- and seven-member rings.[16)]

In this letter, we have studied the effects of lattice vacancies on transport in carbon nanotubes. In the case of vacancy I consisting of a single site, the conductance at $\epsilon = 0$ becomes half that in a perfect nanotube independent of the radius. In the case of vacancy IV consisting of four sites, the conductance vanishes at $\epsilon = 0$. In the case of the vacancy II consisting of a pair of A and B lattices, the conductance stays almost equal to $2e^2/\pi\hbar$ particularly in nanotubes with a sufficiently large radius. This strong dependence on the kind of vacancy prevails even in a magnetic field perpendicular to the axis. A peculiar feature is the existence of the universal dependence on the field component in the direction of the vacancy. In order to reach full understanding of the effects of vacancies, further elaborate calculations should be performed for many different kinds of vacancies. An analytic treatment in an effective-mass approximation should also be useful. These problems are left for a future study.

Acknowledgments

One of the authors (M.I.) is grateful to M. Fujita, K. Nakada, and K. Wakabayashi for their helpful discussions. This work was supported in part by a Grant-in-Aid for Scientific Research from the Ministry of Education, Science, Sports and Culture, Japan. One of us (T.N.) acknowledges the support of a fellowship from the Special Postdoctoral Researches Program at RIKEN. Numerical calculations were performed in part on FACOM VPP500 at the Supercomputer Center, Institute for Solid State Physics, University of Tokyo.

1) S. Iijima: Nature (London) **354** (1991) 56.
2) R. Saito, M. Fujita, G. Dresselhaus and M. S. Dresselhaus: Appl. Phys. Lett. **60** (1992) 2204.
3) R. Saito, M. Fujita, G. Dresselhaus and M. S. Dresselhaus: Phys. Rev. B **46** (1992) 1804.
4) N. Hamada, S. Sawada and A. Oshiyama: Phys. Rev. Lett. **68** (1992) 1579.
5) H. Ajiki and T. Ando: J. Phys. Soc. Jpn. **62** (1993) 1255.
6) T. Ando and T. Nakanishi: J. Phys. Soc. Jpn. **67** (1998) 1704.
7) T. Ando, T. Nakanishi and R. Saito: J. Phys. Soc. Jpn. **67** (1998) 2857.
8) T. Nakanishi and T. Ando: J. Phys. Soc. Jpn. **68** (1999) No. 2.
9) S. N. Song, X. K. Wang, R. P. H. Chang and J. B. Ketterson: Phys. Rev. Lett. **72** (1994) 697.
10) L. Langer, V. Bayot, E. Grive, J.-P. Issi, J. P. Heremans, C. H. Olk, L. Stockman, C. Van Haesendonck and Y. Brunseraede: Phys. Rev. Lett. **76** (1996) 479.
11) F. Katayama: Master Thesis, University of Tokyo, Tokyo, 1996.
12) S. Frank, P. Poncharal, Z. L. Wang and W. A. de Heer: Science **280** (1998) 1744.
13) O. Zhou, R. M. Fleming, D. W. Murphy, R. C. Haddon, A. P. Ramirez and S. H. Glarum: Science **263** (1994) 1744.
14) S. Amelinckx, D. Bernaerts, X. B. Zhang, G. Van Tendeloo and J. Van Landuyt: Science **267** (1995) 1334.
15) R. Tamura and M. Tsukada: Phys. Rev. B **55** (1997) 4991.
16) T. Nakanishi and T. Ando: J. Phys. Soc. Jpn. **66** (1997) 2973.
17) H. Matsumura and T. Ando: J. Phys. Soc. Jpn. **67** (1998) 3542.
18) L. Chico, L. X. Benedict, S. G. Louie and M. L. Cohen: Phys. Rev. B **54** (1996) 2600.
19) H. Ajiki and T. Ando: J. Phys. Soc. Jpn. **65** (1996) 505.
20) R. Saito, G. Dresselhaus and M. S. Dresselhaus: Phys. Rev. B **50** (1994) 14698 [Erratum] Phys. Rev. B **53** (1996) 10408.
21) H. Ajiki and T. Ando: J. Phys. Soc. Jpn. **62** (1993) 2470.
22) T. Seri and T. Ando: J. Phys. Soc. Jpn. **66** (1997) 169.
23) T. Ando and T. Seri: J. Phys. Soc. Jpn. **66** (1997) 3558.
24) T. Ando: Phys. Rev. B **44** (1991) 8017.
25) A. MacKinnon: Z. Phys. B - Condensed Matter **59** (1985) 385.
26) R. Landauer: IBM J. Res. Dev. **1** (1957) 223; Philos. Mag. **21** (1970) 863.
27) M. Fujita, K. Wakabayashi, K. Nakada and K. Kusakabe: J. Phys. Soc. Jpn. **65** (1996) 1920.
28) K. Nakada, M. Fujita, G. Dresselhaus and M. S. Dresselhaus: Phys. Rev. B **54** (1996) 17954.
29) M. Fujita, M. Igami and K. Nakada: J. Phys. Soc. Jpn. **66** (1997) 1864.
30) M. Igami, M. Fujita and S. Mizuno: Appl. Surf. Sci. **130–132** (1998) 870.